

Doping evolution of spin excitations in $\text{La}_{3-x}\text{Sr}_x\text{Ni}_2\text{O}_7/\text{SrLaAlO}_4$ superconducting thin films

Hengyang Zhong^{§,1}, Bo Hao^{§,2,3}, Anni Chen,⁴ Xinru Huang,¹ Chunyi Li,¹ Wenting Zhang,¹ Chang Liu,¹ Kurt Kummer,⁵ Nicholas Brookes,⁵ Yuefeng Nie,^{2,3,6,*} Thorsten Schmitt,^{4,†} and Xingye Lu^{1,‡}

¹Center for Advanced Quantum Studies, School of Physics and Astronomy, and Key Laboratory of Multiscale Spin Physics (Ministry of Education), Beijing Normal University, Beijing 100875, China

²National Laboratory of Solid State Microstructures, Jiangsu Key Laboratory of Artificial Functional Materials, College of Engineering and Applied Sciences, Nanjing University, Nanjing 210093, China

³Collaborative Innovation Center of Advanced Microstructures, Nanjing University, Nanjing 210093, China

⁴Photon Science Division, Swiss Light Source, Paul Scherrer Institut, CH-5232 Villigen PSI, Switzerland

⁵European Synchrotron Radiation Facility, BP 220, F-38043 Grenoble Cedex, France

⁶Jiangsu Physical Science Research Center, Nanjing 210093, China

(Dated: March 3, 2026)

Ambient-pressure superconductivity in compressively strained bilayer nickelate films enables direct spectroscopic tests of pairing scenarios, yet how magnetism evolves with carrier doping remains largely unexplored. Here we use Ni L_3 -edge resonant inelastic x-ray scattering (RIXS) to track electronic and spin excitations in coherently strained $\text{La}_{3-x}\text{Sr}_x\text{Ni}_2\text{O}_7/\text{SrLaAlO}_4$ thin films ($x = 0, 0.09, 0.21$ and 0.38), spanning superconducting and overdoped non-superconducting regimes at essentially fixed epitaxial strain. Transport confirms superconductivity for $x \leq 0.21$ and a weakly insulating normal state at $x = 0.38$. The dd -excitation manifold evolves weakly up to $x = 0.21$, whereas the ~ 0.4 eV and ~ 1.6 eV features broaden and lose intensity at $x = 0.38$. In the superconducting films, dispersive spin excitations persist along both $[H, H]$ and $[H, 0]$ with nearly doping-independent undamped dispersions and only a modest reduction of spectral weight, consistent with robust double-stripe correlations. By contrast, at $x = 0.38$ the magnetic response becomes strongly broadened and weakened, with enhanced damping and $\sim 50\%$ lower spectral weight, indicating a collapse of coherent double-stripe spin excitations. The concomitant suppression of magnetic coherence and superconductivity establishes a direct doping-controlled link between magnetism and superconductivity in bilayer nickelate films.

The discovery of hydrostatic-pressure induced superconductivity in the bilayer Ruddlesden–Popper nickelate $\text{La}_3\text{Ni}_2\text{O}_7$ ($T_{c,\text{onset}} \sim 80$ K) has opened a new avenue for exploring high- T_c superconductivity beyond cuprates and iron-based superconductors [1–5]. Through isovalent rare-earth (such as Pr, Sm, Nd) substitution of La in $\text{La}_3\text{Ni}_2\text{O}_7$ [6–10], the bulk superconductivity can be stabilized and further enhanced to $T_{c,\text{onset}} \sim 96$ K [7]. $\text{La}_3\text{Ni}_2\text{O}_7$ consists of NiO_2 bilayers coupled via inner apical oxygens (O_{AP}), hosting quasi-degenerate Ni $3d_{x^2-y^2}$ and $3d_{z^2}$ orbitals near the Fermi level [1, 11–22] and sizable interlayer superexchange interactions [21, 23–26] in a double-stripe ground state [27–30]. Theoretical and experimental works have emphasized the importance of interlayer antiferromagnetic (AFM) superexchange J_z and spin fluctuations in driving superconductivity in this multi-orbital system [21, 22, 24–26, 31–44]. However, the $P \gtrsim 10$ GPa hydrostatic pressure severely limits systematic spectroscopic probes of the pairing interaction and complicate application-oriented characterization.

Recently, compressive epitaxy on $\text{SrLaAlO}_4(001)$ (SLAO), imposing an in-plane strain of $\varepsilon \approx -2\%$, has been shown to stabilize ambient-pressure superconductivity in $\text{La}_3\text{Ni}_2\text{O}_7$ -based thin films with $T_{c,\text{onset}}$ exceeding 40 K [45–48] and reaching ~ 60 K in the most recent reports [49]. These epitaxial films provide experimental access to momentum- and energy-resolved spectroscopies that are central to unveiling the pairing mechanism [13, 31, 50–52]. Scanning tunneling microscopy/spectroscopy on $\text{La}_2\text{PrNi}_2\text{O}_7/\text{SLAO}$ reveals a fully opened superconducting gap with two characteristic energy scales and a bosonic-mode feature at ~ 30 meV

[50]. Complementary ARPES measurements on superconducting $(\text{La,Pr,Sm})_3\text{Ni}_2\text{O}_7/\text{SLAO}$ resolve a nodeless superconducting gap ($\Delta \approx 18$ meV) and an electron–boson coupling scale, consistent with an s -wave–type order parameter [51]. In parallel, our prior Ni L_3 -edge RIXS study on $\text{La}_3\text{Ni}_2\text{O}_7/\text{SLAO}$ (LNO/SLAO) thin films uncovered robust, dispersive magnetic excitations with collinear double-stripe correlations and enhanced interlayer exchange J_z under compressive strain [31]. Taken together, the spectroscopic evidence for a fully gapped superconducting state and strong antiferromagnetic spin fluctuations is compatible with a spin-fluctuation-mediated s^\pm pairing scenario in bilayer nickelate films [24, 32, 34, 39, 42, 53–60].

However, though dispersive spin excitations were observed in LNO/SLAO thin film, an unambiguous link between superconductivity and spin correlations remains to be explored experimentally [31]. In cuprates and iron-based superconductors, a decisive strategy is to track the evolution of spin excitations with carrier doping across the superconducting phase diagram and into the overdoped, non-superconducting regime [61–64]. The coherently strained $\text{La}_{3-x}\text{Sr}_x\text{Ni}_2\text{O}_7/\text{SLAO}$ (LSNO/SLAO) superconducting thin films (Fig. 1a) provide precisely this opportunity: Sr substitution tunes the carrier density and drives superconductivity from a robust regime ($x \lesssim 0.21$) to a non-superconducting state near $x \approx 0.38$ at essentially fixed epitaxial strain [48, 65].

In this work, we use Ni- L_3 -edge RIXS to track the evolution of magnetic excitations in coherently compressively strained $\text{La}_{3-x}\text{Sr}_x\text{Ni}_2\text{O}_7/\text{SLAO}$ thin films with $x = 0, 0.09, 0.21$, and 0.38 , spanning the superconducting regime ($x \leq$

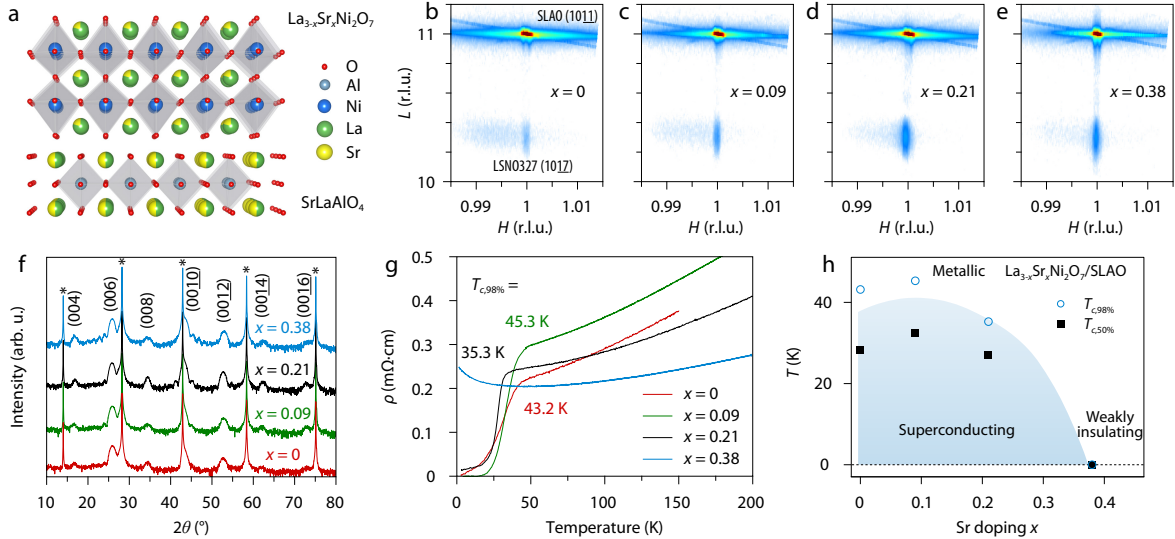


FIG. 1. Epitaxial growth and superconducting phase diagram of $\text{La}_{3-x}\text{Sr}_x\text{Ni}_2\text{O}_7$ thin films on SrLaAlO_4 . **a**, Structural schematic of the $\text{La}_{3-x}\text{Sr}_x\text{Ni}_2\text{O}_7$ (LSNO327) film coherently grown on a (001)-oriented SrLaAlO_4 (SLAO) substrate. **b–e**, Reciprocal space maps in $[H, 0, L]$ plane (in reciprocal lattice units) collected around the SLAO (1011) reflection showing the LSNO327 (1017) film peak for $x = 0$ (b), 0.09 (c), 0.21 (d) and 0.38 (e); the vertical alignment of the film and substrate peaks indicates coherent in-plane strain. **f**, X-ray diffraction $\theta - 2\theta$ scans showing (00L) reflections of the LSNO327 phase (indexed) for films with $x = 0, 0.09, 0.21$ and 0.38 ; asterisks denote substrate-related peaks. **g**, Temperature dependence of the in-plane resistivity $\rho(T)$ for representative films, highlighting superconducting transitions with $T_{c,98\%} = 43.2$ K ($x = 0$), 45.3 K ($x = 0.09$) and 35.3 K ($x = 0.21$), while the $x = 0.38$ film shows weakly insulating behaviour; $T_{c,98\%}$ is defined at 98% of the normal-state resistivity. **h**, Sr-doping evolution of the phase diagram summarizing $T_{c,98\%}$ (open circles) and $T_{c,50\%}$ (solid squares; midpoint criterion). The shaded region marks the superconducting regime.

0.21) and an overdoped, non-superconducting composition ($x = 0.38$) (Fig. 1). With increasing x , the ~ 0.4 and ~ 1.6 eV dd features weaken and, for $x = 0.38$, become strongly broadened and suppressed. Since the ~ 0.4 eV mode is a bilayer e_g -sector excitation that is sensitive to apical-oxygen-mediated interlayer hopping [23], and the ~ 1.6 eV feature lies in a mixed dd /charge-transfer manifold with appreciable ligand-hole character [31], this evolution is consistent with degraded interlayer coherence in the overdoped film. Concomitantly, while the low-energy magnetic response remains robust and dispersive in $x \leq 0.21$, with nearly doping-independent undamped dispersions and a modest reduction of spectral weight, the spin excitations at $x = 0.38$ soften and become strongly damped, accompanied by a pronounced collapse of dispersive spin excitations. The concomitant loss of superconductivity and collapse of coherent double-stripe spin excitations at $x = 0.38$ establishes a direct, doping-controlled link between magnetic coherence and superconductivity in LSNO/SLAO thin films.

Results

Sample and experimental setup

$\text{La}_{3-x}\text{Sr}_x\text{Ni}_2\text{O}_7$ thin films used in this work were epitaxially grown on (001)-oriented SrLaAlO_4 (SLAO) substrates by reactive molecular-beam epitaxy (MBE) in a DCA R450 system [48]. During deposition, the substrate temperature was maintained at ~ 720 °C under a distilled-ozone background

pressure of $\sim 1 \times 10^{-5}$ Torr. Film thickness was precisely controlled by shuttered layer-by-layer growth (monitored by RHEED oscillations) to 3 unit cells to avoid strain relaxation. After growth, the samples were cooled to room temperature under the same oxidizing background to minimize oxygen loss, followed by an ex situ ozone-assisted anneal (typically ~ 380 °C for ~ 1 h) to optimize superconductivity. High crystalline quality and coherent epitaxial strain were confirmed by reciprocal-space mapping (Fig. 1b-1e) and X-ray diffraction $\theta - 2\theta$ scans (Fig. 1f) using monochromated $\text{Cu K}\alpha_1$ radiation. X-ray absorption spectroscopy (XAS) and RIXS measurements were performed at the ID32 beamline of the European Synchrotron Radiation Facility (ESRF). All data shown were collected at $T \approx 20$ K. XAS measurements were performed using total fluorescence yield (TFY) detection. Incident energy dependent RIXS spectra were collected using π -polarized photons. Momentum-dependent RIXS spectra were collected at the Ni-L_3 edge (856.4 eV) using π -polarized incident photons along two high-symmetry directions $[H, 0]$ and $[H, H]$, under the grazing-incidence geometry, with an energy resolution $\Delta E \approx 32$ meV.

Figure 1g plots the temperature-dependent in-plane resistivity $\rho(T)$ of LSNO/SLAO films. Using the 98% criterion, the superconducting onsets are $T_{c,98\%} = 43.2$ K ($x = 0$), 45.3 K ($x = 0.09$), and 35.3 K ($x = 0.21$); by contrast, the $x = 0.38$ film remains metallic for $T \gtrsim 50$ K but develops a low- T resistivity upturn, consistent with a weakly insulating response.

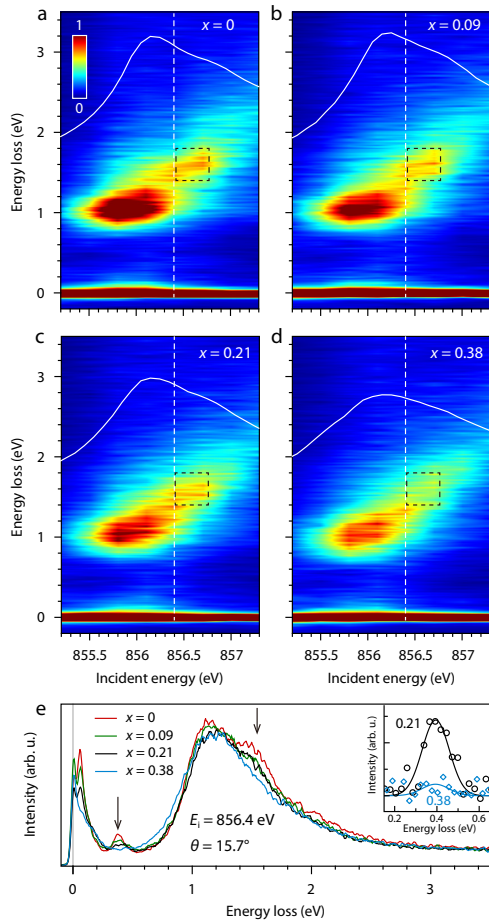


FIG. 2. Sr-doping evolution of dd excitations in LSNO/SLAO thin films. **a–d**, Incident-energy-dependent Ni- L_3 RIXS intensity maps measured at a grazing-incidence angle $\theta = 20^\circ$ for films with $x = 0$ (**a**), 0.09 (**b**), 0.21 (**c**) and 0.38 (**d**), plotted as a function of incident photon energy (E_i) and energy loss. The solid white curves show the corresponding Ni- L_3 X-ray absorption spectra (scaled for clarity). The black dashed squares mark the ~ 1.6 eV dd excitations. The vertical dashed line marks $E_i = 856.4$ eV, the incident energy used to extract the spectra in **e**. **e**, Comparison of Ni- L_3 RIXS spectra measured at $E_i = 856.4$ eV and a grazing-incidence angle $\theta = 15.7^\circ$ for the four dopings, highlighting the doping-dependent evolution of the dd excitations; vertical arrows indicate the changes of the ~ 0.4 eV and ~ 1.6 eV features. Data for $x = 0$ are from Ref. [31]. The inset in **e** shows a comparison of the 0.4 eV excitation between $x = 0.21$ and 0.38.

Figure 1h summarizes $T_{c,98\%}$ and $T_{c,50\%}$ versus Sr content, reproducing the incomplete dome reported in Ref. [48]: superconductivity persists up to $x \approx 0.21$ and is absent down to 2 K at $x = 0.38$.

Doping evolution of electronic and spin excitations

Figure 2 summarizes the incident-energy-dependent Ni- L_3 RIXS response of LSNO/SLAO across the Sr-doping series. The overall dd manifold remains broadly similar for $x \leq 0.21$ (Fig. 2a-c, e). In this doping range, the ~ 0.4 eV excitation remains resolvable as a peak (becoming broader and reduced

in contrast at $x = 0.21$), and the ~ 1.6 eV feature can be identified as a broad shoulder/peak-like enhancement on the high-energy slope (Fig. 2e). In the overdoped $x = 0.38$ film, the ~ 0.4 eV response becomes essentially featureless (Fig. 2d,e), and the ~ 1.6 eV shoulder is no longer discernible, indicating a marked loss of well-defined orbital-excitation structure in this energy window.

This trend is naturally interpreted in terms of degraded bilayer (interlayer) coherence in the overdoped regime. In the double-cluster (bilayer) description, the ~ 0.4 eV mode has been assigned to transitions between $d_{x^2-y^2}$ and d_{z^2} , with its energy governed primarily by interlayer hopping [23]. It carries mixed charge/spin character and is particularly sensitive to apical-oxygen-mediated interlayer hopping; its strong broadening and disappearance at $x = 0.38$ is consistent with a substantial loss of interlayer coherence. The simultaneous suppression of the ~ 1.6 eV feature, which lies in a mixed dd /charge-transfer manifold with appreciable ligand-hole character, supports the same conclusion that bilayer coherence is strongly degraded in the overdoped film.

Having established that Sr doping progressively weakens and broadens the ~ 0.4 and ~ 1.6 eV orbital-excitation features—consistent with degraded bilayer coherence in the overdoped film—we now turn to the low-energy magnetic response. To directly track how spin correlations evolve across a doping-tuned thin-film phase diagram at essentially fixed epitaxial strain, we performed momentum-resolved Ni L_3 -edge RIXS measurements (π polarization, grazing-incidence geometry; $\Delta E \approx 32$ meV) on $\text{La}_{3-x}\text{Sr}_x\text{Ni}_2\text{O}_7/\text{SLAO}$ films at the same Sr concentrations as in Fig. 2 ($x = 0, 0.09, 0.21,$ and 0.38). The scattering angle was set to $2\theta_s = 90^\circ$ and 110° to reduce the elastic scattering. These measurements provide a direct basis for comparing the coherence, dispersion, and spectral weight of collective spin excitations between the superconducting and overdoped non-superconducting regimes (Fig. 3).

Figure 3 provides a direct visualization of the Sr-doping evolution of spin excitations in LSNO/SLAO films. The RIXS intensity maps in Fig. 3a–c show a well-defined, dispersive magnetic mode for all superconducting compositions ($x = 0, 0.09,$ and 0.21) along both high-symmetry directions, $[H, H]$ and $[H, 0]$. For $x = 0$, Fig. 3a is dominated by a well-defined collective magnetic mode that reaches its maximum near the zone center Γ and disperses downward to a minimum around $\mathbf{q}_{\parallel} \approx (1/4, 1/4)$, consistent with robust collinear (double-stripe–like) spin correlations [31]. Importantly, for $x = 0.09$ and 0.21 (Fig. 3b,c), the dispersive features remain clearly resolved and the fitted undamped dispersions $E_0(\mathbf{q}_{\parallel})$ are essentially unchanged compared with $x = 0$, indicating that the underlying collinear double-stripe spin correlations and their characteristic exchange scale persist across the superconducting regime, with only a modest reduction of spectral weight.

In sharp contrast, the overdoped non-superconducting $x = 0.38$ film (Fig. 3d) exhibits a qualitatively different magnetic response—the excitation spectrum becomes strongly broadened and continuum-like, and the dispersive peak is no longer

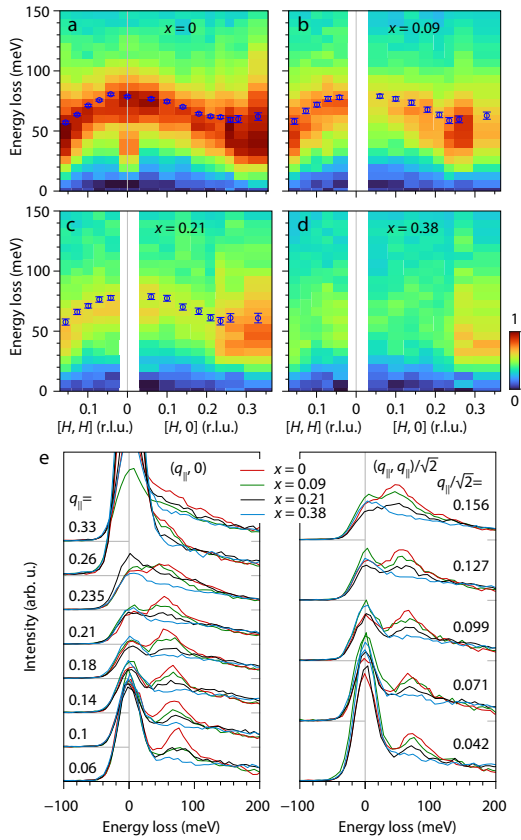


FIG. 3. Sr-doping evolution of spin excitations in LSNO/SLAO thin films. **a–d**, False-colour maps of the low-energy Ni- L_3 RIXS intensity plotted as a function of energy loss and in-plane momentum transfer \mathbf{q}_{\parallel} along the $[H, H]$ direction (left part of each panel) and the $[H, 0]$ direction (right part), for $x = 0$ (**a**), 0.09 (**b**), 0.21 (**c**) and 0.38 (**d**). Elastic scattering has been fitted and subtracted from the color maps. The scattering angle $2\theta_s = 110^\circ$ for $|\mathbf{q}_{\parallel}| \geq 0.26$ and $2\theta_s = 90^\circ$ otherwise. The symbols overlaid on the maps denote the undamped spin-excitation dispersion $E_0(\mathbf{q}_{\parallel})$ extracted from fits to the RIXS spectra (error bars indicate fitting uncertainties). **e**, Waterfall plots of representative low-energy Ni- L_3 RIXS spectra measured with π -polarized incident X-rays at $T \approx 20$ K for $x = 0, 0.09, 0.21$ and 0.38, along $(\mathbf{q}_{\parallel}, 0)$ (left) and $(\mathbf{q}_{\parallel}, \mathbf{q}_{\parallel})/\sqrt{2}$ (right); spectra are vertically offset for clarity and \mathbf{q}_{\parallel} values are indicated. Dispersive, well-defined spin excitations persist up to $x = 0.21$, whereas for $x = 0.38$ the magnetic response is strongly broadened and its intensity is markedly reduced over the entire measured \mathbf{q}_{\parallel} range. Data for $x = 0$ are from Ref. [31].

clearly resolved over the measured \mathbf{q}_{\parallel} range, and accompanied by a pronounced loss of spectral weight. The doping evolution is most transparent in the \mathbf{q}_{\parallel} -dependent waterfall comparison in Fig. 3(e). For $x \leq 0.21$, the spectra display pronounced magnon-like peaks that disperse with momentum, whereas for $x = 0.38$ the response is dominated by broad intensity with greatly reduced peak contrast. Taken together, these data show that the coherent double-stripe spin excitations are robust throughout the superconducting compositions but collapse in the overdoped non-superconducting film, establishing a direct doping-controlled link between magnetic coherence

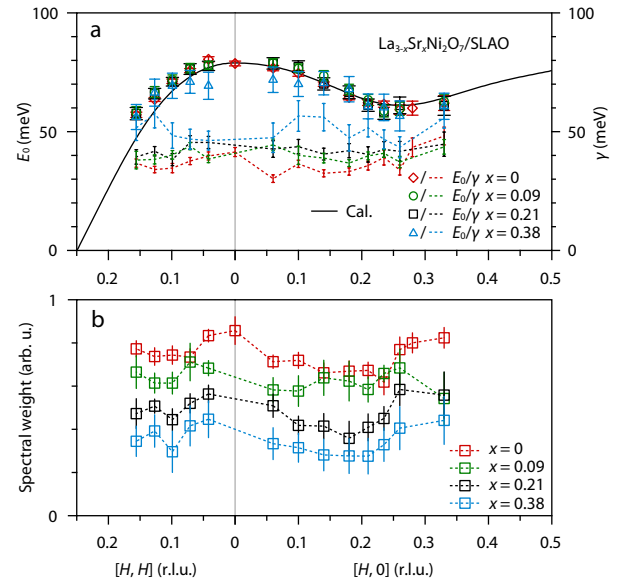


FIG. 4. Dispersions, damping and spectral weight of spin excitations across Sr doping in LSNO/SLAO thin films. **a**, Undamped spin-excitation energy $E_0(\mathbf{q}_{\parallel})$ (symbols; left axis) and damping factor $\gamma(\mathbf{q}_{\parallel})$ (data points connected by dashed lines; right axis) extracted from damped-harmonic-oscillator (DHO) fits to the low-energy Ni- L_3 RIXS spectra for $x = 0, 0.09, 0.21$ and 0.38, plotted along the $[H, H]$ (left) and $[H, 0]$ (right) directions. The vertical grey line marks Γ ($\mathbf{q}_{\parallel} = 0$), and the solid black curve shows the fitted dispersion for comparison. For $x \leq 0.21$, the dispersions nearly coincide and the modes remain weakly damped, whereas for $x = 0.38$ the dispersion softens and the damping increases markedly over the full \mathbf{q}_{\parallel} range. **b**, Momentum dependence of the magnon spectral weight $W(\mathbf{q}_{\parallel})$, obtained by energy integration of the fitted DHO lineshapes. Error bars in **a**, **b** represent uncertainties from the fits; dashed lines are guides to the eye.

and superconductivity in bilayer nickelate films.

To quantify the doping evolution of the spin excitations. We use a damped-harmonic-oscillator (DHO) response function to fit the low-energy part of each Ni- L_3 RIXS spectrum to extract the momentum-dependent spin excitations [66]: $S(\mathbf{q}, E) = A \frac{4\gamma E E_0}{(E^2 - E_0^2)^2 + (2\gamma E)^2}$ where $E_0(\mathbf{q})$ is the undamped mode energy and $\gamma(\mathbf{q})$ characterizes the damping (linewidth). The prefactor A sets the overall intensity of the magnetic response; the magnetic spectral weight is obtained from the integrated area of the fitted DHO component (within the chosen energy window), while $E_0(\mathbf{q})$ directly yields the fitted dispersion.

Figure 4 quantifies the doping evolution of the magnetic mode by tracking the fitted undamped dispersion $E_0(\mathbf{q}_{\parallel})$ and damping $\gamma(\mathbf{q}_{\parallel})$ extracted from the DHO analysis. For the superconducting compositions measured here ($x = 0, 0.09, 0.21$), the RIXS spectra exhibit well-defined magnon-like peaks (Fig. 3a-c), making the extracted E_0 and γ reliable. The dispersions for $x \leq 0.21$ are essentially coincident along both $[H, H]$ and $[H, 0]$, providing a quantitative confirmation that the characteristic double-stripe spin corre-

lations and their underlying exchange scale persist across this high- T_c portion of the superconducting dome. Consistent with our previous double-stripe analysis, the dispersion can be described by linear spin-wave calculations of a classical Heisenberg model $H = \sum_{i<j} J_{ij} \mathbf{S}_i \cdot \mathbf{S}_j$ (SpinW), yielding exchange parameters $SJ_1 \approx -8.0$ meV, $SJ_2 \approx -3.7$ meV, and a dominant $SJ_z \approx 44.4$ meV for $x = 0 - 0.21$ (black curve in Fig. 4a). The corresponding damping remains modest in this doping range (Fig. 4b), consistent with well-defined collective spin excitations in the superconducting compositions.

For the overdoped, non-superconducting $x = 0.38$ film, the magnetic response is strongly broadened and continuum-like (Fig. 3d), so extracting a unique collective-mode dispersion is intrinsically less constrained. To estimate an *upper bound* on any remaining coherent component, we fit the spectra using the same DHO form (with a constrained bimagnon continuum) and test consistency with the double-stripe Heisenberg description. Under this procedure, Fig. 4a indicates a modest softening of the band top by $\sim 10 - 12$ meV, corresponding to reduced effective exchanges $SJ_1 \approx -5.5$ meV, $SJ_2 \approx -2.6$ meV, and $SJ_z \approx 35.2$ meV, together with a pronounced enhancement of $\gamma(\mathbf{q}_{\parallel})$ relative to $x \leq 0.21$ (Fig. 4b). Meanwhile, the integrated magnetic spectral weight decreases smoothly with Sr content (Fig. 4b) and is $\sim 50\%$ lower at $x = 0.38$ than at $x = 0$. Given the lack of a clearly resolved dispersive peak in Fig. 3d, these $x = 0.38$ parameters should be viewed as a highest estimate; the data are also consistent with the coherent (magnon-like) component being essentially quenched, leaving a predominantly incoherent continuum.

Discussion

In cuprates and iron-based superconductors, magnetic excitations span a broad hierarchy of energies and encode complementary aspects of the pairing problem. The high-energy spin excitations (paramagnons/spin waves) mainly reflect the persistence of spin correlations (J), which is suggested to serve as a pairing interaction in spin-fluctuation pairing theories [61–64]. The low-energy sector is strongly shaped by itinerant electrons and often shows the most direct fingerprints of superconductivity, including the appearance of a superconductivity-induced spin-resonance mode and a pronounced doping dependence of the low-energy spectral weight [63, 64, 67, 68]. Tracking how these spin excitations evolve across the superconducting dome, especially into the overdoped regime where superconductivity vanishes, has therefore been a decisive experimental strategy for establishing a link between magnetism and pairing in both families [61–64].

Our results place Sr-doped bilayer nickelate films squarely into this comparative framework, but with a distinctive outcome. In the superconducting compositions measured here ($x = 0, 0.09, 0.21$), the collective magnetic mode remains well-defined and strongly dispersive, and the extracted undamped dispersions are essentially unchanged, consistent with the persistence of double-stripe spin correlations in the high- T_c portion of the dome. A double-stripe Heisenberg

description yields representative exchange parameters $SJ_1 \approx -8.0$ meV, $SJ_2 \approx -3.7$ meV, $SJ_z \approx 44.4$ meV, while the spectral weight decreases only gradually and the modes remain in the underdamped regime. In the overdoped, non-superconducting $x = 0.38$ film, the response becomes strongly broadened and continuum-like, and even under a conservative fitting procedure the inferred exchanges are significantly reduced ($SJ_1 \approx -5.5$ meV, $SJ_2 \approx -2.6$ meV, $SJ_z \approx 35.2$ meV) with a pronounced enhancement of damping; simultaneously, the integrated magnetic spectral weight is reduced to $\sim 50\%$ of that at $x = 0$. It is reminiscent of $\text{La}_3\text{Ni}_2\text{O}_7/\text{SrTiO}_3$ films, where both the ~ 1.6 eV excitation and the low-energy magnetic response are strongly suppressed under tensile strain, consistent with weakened Ni $3d_{z^2}$ - $\text{O}_{\text{AP}} 2p_z$ hybridization and a reduced interlayer superexchange scale J_z [31]. In the present overdoped films, the concurrent loss of well-defined ~ 0.4 eV and ~ 1.6 eV orbital-excitation features points to degraded apical-oxygen-mediated bilayer coherence/hybridization, which in turn is accompanied by a substantially broadened, low-spectral-weight magnetic continuum. The collapse (and possible quenching) of coherent double-stripe spin excitations together with the disappearance of superconductivity therefore establishes a direct, doping-controlled correlation between magnetic coherence and superconductivity in $\text{La}_{3-x}\text{Sr}_x\text{Ni}_2\text{O}_7$ films, which is more stringent than in systems where high-energy paramagnons remain robust even after superconductivity is suppressed [62, 69].

Looking forward, bilayer nickelate films offer an unusually favorable geometry for momentum-resolved “phase-diagram spectroscopy” with soft x-ray RIXS. The characteristic double-stripe wave vector near $\mathbf{q} \approx (1/4, 1/4)$ lies well within the momentum window of Ni L_3 RIXS, making $\text{La}_3\text{Ni}_2\text{O}_7$ -based films a rare system among high- T_c superconductors, in which both the ordering wave vector and its collective excitations can be mapped directly at the corresponding transition-metal L_3 edge. With the new generation RIXS with energy resolution approaching ~ 10 meV, it should become feasible to search for a superconductivity-induced spin resonance in the $\sim 15 - 25$ meV range (using the empirical scaling $E_r \sim 4 - 6 k_B T_c$, which gives $E_r \sim 20$ meV for $T_c \sim 50$ K) [68]. Detecting such a mode and tracking its intensity with Sr doping alongside the damping and spectral weight trends established here would provide an exceptionally direct test of sign-changing pairing (e.g., s^{\pm}) and offer unprecedented constraints on the pairing interaction in bilayer nickelate superconductors.

Author contributions

X.L., T.S., and Y.N. conceived this project. B.H. grew the thin films and did the transport and x-ray diffraction measurements. H.Z., A.C., X.H., C.Li., W.Z., C.Liu. and X.L. performed the RIXS experiments with the help from K.K. and N.B.. H.Z., A.C. and X.L. analysed the data. X.L. wrote the manuscript with inputs from H.Z., B.H., Y.N. and T.S.. All authors made comments.

Acknowledgement

§ These two authors contributed equally to this work.

The work is supported by the Scientific Research Innovation Capability Support Project for Young Faculty (ZYGXQNJSKYCXNLZCXM-M2), the National Natural Science Foundation of China (Grants no. 12574142, and 12434002), National Key Projects for Research and Development of China with Grant No. 2021YFA1400400 and Natural Science Foundation of Jiangsu Province (No. BK20233001). The work at PSI is supported by the Swiss National Science Foundation through project No. 207904. We acknowledge the European Synchrotron Radiation Facility (ESRF) for providing synchrotron radiation facilities under proposal numbers SC-5699 at the ID32 beamline.

* ynie@nju.edu.cn

† thorsten.schmitt@psi.ch

‡ luxy@bnu.edu.cn

- [1] H. Sun, M. Huo, X. Hu, J. Li, Z. Liu, Y. Han, L. Tang, Z. Mao, P. Yang, B. Wang, J. Cheng, D.-X. Yao, G.-M. Zhang, and M. Wang, Signatures of superconductivity near 80 K in a nickelate under high pressure, *Nature* **621**, 493 (2023).
- [2] Y. Zhang, D. Su, Y. Huang, Z. Shan, H. Sun, M. Huo, K. Ye, J. Zhang, Z. Yang, Y. Xu, Y. Su, R. Li, M. Smidman, M. Wang, L. Jiao, and H. Yuan, High-temperature superconductivity with zero resistance and strange-metal behaviour in $\text{La}_3\text{Ni}_2\text{O}_{7-\delta}$, *Nat. Phys.* **20**, 1269–1273 (2024).
- [3] G. Wang, N. N. Wang, X. L. Shen, J. Hou, L. Ma, L. F. Shi, Z. A. Ren, Y. D. Gu, H. M. Ma, P. T. Yang, Z. Y. Liu, H. Z. Guo, J. P. Sun, G. M. Zhang, S. Calder, J.-Q. Yan, B. S. Wang, Y. Uwatoko, and J.-G. Cheng, Pressure-induced superconductivity in polycrystalline $\text{La}_3\text{Ni}_2\text{O}_{7-\delta}$, *Phys. Rev. X* **14**, 011040 (2024).
- [4] M. Shi, D. Peng, Y. Li, S. Yang, Z. Xing, Y. Wang, K. Fan, H. Li, R. Wu, B. Ge, Z. Zeng, Q. Zeng, J. Ying, T. Wu, and X. Chen, Spin density wave rather than tetragonal structure is prerequisite for superconductivity in $\text{La}_3\text{Ni}_2\text{O}_{7-\delta}$, *Nature Communications* **16**, 9141 (2025).
- [5] J. Li, D. Peng, P. Ma, H. Zhang, Z. Xing, X. Huang, C. Huang, M. Huo, D. Hu, Z. Dong, X. Chen, T. Xie, H. Dong, H. Sun, Q. Zeng, H.-k. Mao, and M. Wang, Identification of the superconductivity in bilayer nickelate $\text{La}_3\text{Ni}_2\text{O}_7$ under high pressure up to 100 GPa, *Natl. Sci. Rev.* **12**, nwaf220 (2025).
- [6] N. Wang, G. Wang, X. Shen, J. Hou, J. Luo, X. Ma, H. Yang, L. Shi, J. Dou, J. Feng, J. Yang, Y. Shi, Z. Ren, H. Ma, P. Yang, Z. Liu, Y. Liu, H. Zhang, X. Dong, Y. Wang, K. Jiang, J. Hu, S. Nagasaki, K. Kitagawa, S. Calder, J. Yan, J. Sun, B. Wang, R. Zhou, Y. Uwatoko, and J. Cheng, Bulk high-temperature superconductivity in pressurized tetragonal $\text{La}_2\text{PrNi}_2\text{O}_7$, *Nature* **634**, 579–584 (2024).
- [7] F. Li, Z. Xing, D. Peng, J. Dou, N. Guo, L. Ma, Y. Zhang, L. Wang, J. Luo, J. Yang, J. Zhang, T. Chang, Y.-S. Chen, W. Cai, J. Cheng, Y. Wang, Y. Liu, T. Luo, N. Hiraio, T. Matsuoka, H. Kadobayashi, Z. Zeng, Q. Zheng, R. Zhou, Q. Zeng, X. Tao, and J. Zhang, Bulk superconductivity up to 96 K in pressurized nickelate single crystals, *Nature in press*, <https://doi.org/10.1038/s41586-025-09954-4> (2025).
- [8] Q. Zhong, J. Chen, Z. Qiu, J. Li, X. Huang, P. Ma, M. Huo, H. Dong, H. Sun, and M. Wang, Evolution of the superconductivity in pressurized $\text{La}_{3-x}\text{Sm}_x\text{Ni}_2\text{O}_7$, (2025), [arXiv:2510.13342](https://arxiv.org/abs/2510.13342).
- [9] Z. Qiu, J. Chen, D. V. Semenov, Q. Zhong, D. Zhou, J. Li, P. Ma, X. Huang, M. Huo, T. Xie, X. Chen, H. Kwang Mao, V. Struzhkin, H. Sun, and M. Wang, Interlayer coupling enhanced superconductivity near 100 K in $\text{La}_{3-x}\text{Nd}_x\text{Ni}_2\text{O}_7$, [arXiv:2510.12359](https://arxiv.org/abs/2510.12359).
- [10] Z. Pan, C. Lu, F. Yang, and C. Wu, Effect of rare-earth element substitution in superconducting $\text{R}_3\text{Ni}_2\text{O}_7$ under pressure, *Chinese Phys. Lett.* **41**, 087401 (2024).
- [11] Z. Luo, X. Hu, M. Wang, W. Wú, and D.-X. Yao, Bilayer two-orbital model of $\text{La}_3\text{Ni}_2\text{O}_7$ under pressure, *Phys. Rev. Lett.* **131**, 126001 (2023).
- [12] P. Li, G. Zhou, W. Lv, Y. Li, C. Yue, H. Huang, L. Xu, J. Shen, M. Yu, W. Song, Z. Nie, Y. Chen, H. Wang, W. Chen, Y. Huang, Z.-Y. Chen, Q. Tian, J. Lin, J. He, Y.-J. Sun, Z. Chen, and Q.-K. Xue, Angle-resolved photoemission spectroscopy of superconducting $(\text{La},\text{Pr})_3\text{Ni}_2\text{O}_7/\text{SrLaAlO}_4$ heterostructures, *Natl. Sci. Rev.* **12**, nwaf205 (2025).
- [13] B. Y. Wang, Y. Zhong, S. Abadi, Y. Liu, Y. Yu, X. Zhang, Y.-M. Wu, R. Wang, J. Li, Y. Tarn, E. K. Ko, V. Thampy, M. Hashimoto, D. Lu, Y. S. Lee, T. P. Devereaux, C. Jia, H. Y. Hwang, and Z.-X. Shen, Electronic structure of compressively strained thin film $\text{La}_2\text{PrNi}_2\text{O}_7$, [arXiv:2504.16372](https://arxiv.org/abs/2504.16372).
- [14] Y. Wang, K. Jiang, J. Ying, T. Wu, J. Cheng, J. Hu, and X. Chen, Recent progress in nickelate superconductors, *Natl. Sci. Rev.* **12**, nwaf373 (2025).
- [15] Z. Liu, M. Huo, J. Li, and et al., Electronic correlations and partial gap in the bilayer nickelate $\text{La}_3\text{Ni}_2\text{O}_7$, *Nat. Commun.* **15**, 7570 (2024).
- [16] J. Yang, H. Sun, X. Hu, Y. Xie, T. Miao, H. Luo, H. Chen, B. Liang, W. Zhu, G. Qu, C.-Q. Chen, M. Huo, Y. Huang, S. Zhang, F. Zhang, F. Yang, Z. Wang, Q. Peng, H. Mao, G. Liu, Z. Xu, T. Qian, D.-X. Yao, M. Wang, L. Zhao, and X. J. Zhou, Orbital-dependent electron correlation in double-layer nickelate $\text{La}_3\text{Ni}_2\text{O}_7$, *Nat. Commun.* **15**, 4373 (2024).
- [17] Y. Zhang, L.-F. Lin, A. Moreo, and E. Dagotto, Electronic structure, dimer physics, orbital-selective behavior, and magnetic tendencies in the bilayer nickelate superconductor $\text{La}_3\text{Ni}_2\text{O}_7$ under pressure, *Phys. Rev. B* **108**, L180510 (2023).
- [18] V. Christiansson, F. Petocchi, and P. Werner, Correlated electronic structure of $\text{La}_3\text{Ni}_2\text{O}_7$ under pressure, *Phys. Rev. Lett.* **131**, 206501 (2023).
- [19] F. Lechermann, J. Gondolf, S. Bötzel, and I. M. Eremin, Electronic correlations and superconducting instability in $\text{La}_3\text{Ni}_2\text{O}_7$ under high pressure, *Phys. Rev. B* **108**, L201121 (2023).
- [20] D. A. Shilenko and I. V. Leonov, Correlated electronic structure, orbital-selective behavior, and magnetic correlations in double-layer $\text{La}_3\text{Ni}_2\text{O}_7$ under pressure, *Phys. Rev. B* **108**, 125105 (2023).
- [21] Y. Cao and Y.-f. Yang, Flat bands promoted by Hund’s rule coupling in the candidate double-layer high-temperature superconductor $\text{La}_3\text{Ni}_2\text{O}_7$ under high pressure, *Phys. Rev. B* **109**, L081105 (2024).
- [22] Q. Qin and Y.-F. Yang, High- T_c superconductivity by mobilizing local spin singlets and possible route to higher T_c in pressurized $\text{La}_3\text{Ni}_2\text{O}_7$, *Phys. Rev. B* **108**, L140504 (2023).
- [23] X. Chen, J. Choi, Z. Jiang, J. Mei, K. Jiang, J. Li, S. Agrestini, M. Garcia-Fernandez, H. Sun, X. Huang, D. Shen, M. Wang, J. Hu, Y. Lu, K.-J. Zhou, and D. Feng, Electronic and magnetic excitations in $\text{La}_3\text{Ni}_2\text{O}_7$, *Nat. Commun.* **15**, 9597 (2024).
- [24] C. Lu, Z. Pan, F. Yang, and C. Wu, Interlayer-coupling-driven high-temperature superconductivity in $\text{La}_3\text{Ni}_2\text{O}_7$ under pressure, *Phys. Rev. Lett.* **132**, 146002 (2024).
- [25] Y.-f. Yang, G.-M. Zhang, and F.-C. Zhang, Interlayer valence bonds and two-component theory for high- T_c superconductivity

- ity of $\text{La}_3\text{Ni}_2\text{O}_7$ under pressure, *Phys. Rev. B* **108**, L201108 (2023).
- [26] Y. Shen, M. Qin, and G.-M. Zhang, Effective bi-layer model hamiltonian and density-matrix renormalization group study for the high- T_c superconductivity in $\text{La}_3\text{Ni}_2\text{O}_7$ under high pressure, *Chinese Phys. Lett.* **40**, 127401 (2023).
- [27] I. Plokhikh, T. J. Hicken, L. Keller, V. Pomjakushin, S. H. Moody, P. Foury-Leykian, J. J. Krieger, H. Luetkens, Z. Guguchia, R. Khasanov, and D. J. Gawryluk, Unraveling spin density wave order in layered nickelates $\text{La}_3\text{Ni}_2\text{O}_7$ and $\text{La}_2\text{PrNi}_2\text{O}_7$ via neutron diffraction, [arXiv:2503.05287](https://arxiv.org/abs/2503.05287).
- [28] N. K. Gupta, R. Gong, Y. Wu, M. Kang, C. T. Parzyck, B. Z. Gregory, N. Costa, R. Sutarto, S. Sarker, A. Singer, D. G. Schlom, K. M. Shen, and D. G. Hawthorn, Anisotropic spin stripe domains in bilayer $\text{La}_3\text{Ni}_2\text{O}_7$, *Nat. Commun.* **16**, 6560 (2025).
- [29] X. Ren, R. Sutarto, X. Wu, J. Zhang, H. Huang, T. Xiang, J. Hu, R. Comin, X. Zhou, and Z. Zhu, Resolving the electronic ground state of $\text{La}_3\text{Ni}_2\text{O}_{7-\delta}$ films, *Commun. Phys.* **8**, 52 (2025).
- [30] X.-S. Ni, Y. Ji, L. He, T. Xie, D.-X. Yao, M. Wang, and K. Cao, Spin density wave in the bilayered nickelate $\text{La}_3\text{Ni}_2\text{O}_{7-\delta}$ at ambient pressure, *npj Quantum Mater.* **10**, 17 (2025).
- [31] H. Zhong, B. Hao, Z. Zhang, A. Chen, Y. Wei, R. Liu, X. Huang, C. Li, W. Zhang, C. Liu, X.-S. Ni, M. dos Reis Cantarino, K. Kummer, N. Brookes, K. Cao, Y. Nie, T. Schmitt, and X. Lu, Spin correlations in $\text{La}_3\text{Ni}_2\text{O}_7$ superconducting thin films, [arXiv:2502.03178](https://arxiv.org/abs/2502.03178).
- [32] X.-Z. Qu, D.-W. Qu, J. Chen, C. Wu, F. Yang, W. Li, and G. Su, Bilayer $t-J-J_\perp$ model and magnetically mediated pairing in the pressurized nickelate $\text{La}_3\text{Ni}_2\text{O}_7$, *Phys. Rev. Lett.* **132**, 036502 (2024).
- [33] H. Oh and Y.-H. Zhang, Type-II $t-J$ model and shared superexchange coupling from Hund's rule in superconducting $\text{La}_3\text{Ni}_2\text{O}_7$, *Phys. Rev. B* **108**, 174511 (2023).
- [34] Y.-H. Tian, Y. Chen, J.-M. Wang, R.-Q. He, and Z.-Y. Lu, Correlation effects and concomitant two-orbital s_{\pm} -wave superconductivity in $\text{La}_3\text{Ni}_2\text{O}_7$ under high pressure, *Phys. Rev. B* **109**, 165154 (2024).
- [35] J. Chen, F. Yang, and W. Li, Orbital-selective superconductivity in the pressurized bilayer nickelate $\text{La}_3\text{Ni}_2\text{O}_7$: An infinite projected entangled-pair state study, *Phys. Rev. B* **110**, L041111 (2024).
- [36] Z. Ouyang, J.-M. Wang, J.-X. Wang, R.-Q. He, L. Huang, and Z.-Y. Lu, Hund electronic correlation in $\text{La}_3\text{Ni}_2\text{O}_7$ under high pressure, *Phys. Rev. B* **109**, 115114 (2024).
- [37] C. Lu, M. Zhang, Z. Pan, C. Wu, and F. Yang, Impact of pressure and apical oxygen vacancies on superconductivity in $\text{La}_3\text{Ni}_2\text{O}_7$, *Commun. Phys.* **8**, 354 (2025).
- [38] X.-Z. Qu, D.-W. Qu, X. W. Yi, W. Li, and G. Su, Hund's rule, interorbital hybridization, and high- T_c superconductivity in the bilayer nickelate $\text{La}_3\text{Ni}_2\text{O}_7$, *Phys. Rev. B* **112**, L161101 (2025).
- [39] H. Sakakibara, N. Kitamine, M. Ochi, and K. Kuroki, Possible high T_c superconductivity in $\text{La}_3\text{Ni}_2\text{O}_7$ under high pressure through manifestation of a nearly half-filled bilayer hubbard model, *Phys. Rev. Lett.* **132**, 106002 (2024).
- [40] Z. Luo, B. Lv, M. Wang, W. Wu, D.-X. Yao, and et al., High- T_c superconductivity in $\text{La}_3\text{Ni}_2\text{O}_7$ based on the bilayer two-orbital $t-J$ model, *npj Quantum Mater.* **9**, 61 (2024).
- [41] T. Kaneko, H. Sakakibara, M. Ochi, and K. Kuroki, Pair correlations in the two-orbital Hubbard ladder: Implications for superconductivity in the bilayer nickelate $\text{La}_3\text{Ni}_2\text{O}_7$, *Phys. Rev. B* **109**, 045154 (2024).
- [42] Y.-Y. Zheng and W. Wú, s_{\pm} -wave superconductivity in the bilayer two-orbital hubbard model, *Phys. Rev. B* **111**, 035108 (2025).
- [43] M. Kakoi, T. Kaneko, H. Sakakibara, M. Ochi, and K. Kuroki, Pair correlations of the hybridized orbitals in a ladder model for the bilayer nickelate $\text{La}_3\text{Ni}_2\text{O}_7$, *Phys. Rev. B* **109**, L201124 (2024).
- [44] J. Wang and Y.-f. Yang, Highly asymmetric superconducting dome and strange metallicity in $\text{La}_3\text{Ni}_2\text{O}_7$, *Phys. Rev. B* **111**, 014512 (2025).
- [45] E. K. Ko, Y. Yu, Y. Liu, L. Bhatt, J. Li, V. Thampy, C.-T. Kuo, B. Y. Wang, Y. Lee, K. Lee, J.-S. Lee, B. H. Goodge, D. A. Muller, and H. Y. Hwang, Signatures of ambient pressure superconductivity in thin film $\text{La}_3\text{Ni}_2\text{O}_7$, *Nature* **638**, 935–940 (2024).
- [46] G. Zhou, W. Lv, H. Wang, Z. Nie, Y. Chen, Y. Li, H. Huang, W.-Q. Chen, Y.-J. Sun, Q.-K. Xue, and Z. Chen, Ambient-pressure superconductivity onset above 40 K in $(\text{La,Pr})_3\text{Ni}_2\text{O}_7$ films, *Nature* **640**, 641–646 (2025).
- [47] Y. Liu, E. K. Ko, Y. Tarn, L. Bhatt, J. Li, V. Thampy, B. H. Goodge, D. A. Muller, S. Raghu, Y. Yu, and H. Y. Hwang, Superconductivity and normal-state transport in compressively strained $\text{La}_2\text{PrNi}_2\text{O}_7$ thin films, *Nat. Mater.* **24**, 1221–1227 (2025).
- [48] B. Hao, M. Wang, W. Sun, Y. Yang, Z. Mao, S. Yan, H. Sun, H. Zhang, L. Han, Z. Gu, J. Zhou, D. Ji, and Y. Nie, Superconductivity in Sr-doped $\text{La}_3\text{Ni}_2\text{O}_7$ thin films, *Nat. Mater.* **24**, 1756–1762 (2025).
- [49] G. Zhou, H. Wang, H. Huang, Y. Chen, F. Peng, W. Lv, Z. Nie, W. Wang, Q.-K. Xue, and Z. Chen, Superconductivity onset above 60 K in ambient-pressure nickelate films, [arXiv:2512.04708](https://arxiv.org/abs/2512.04708).
- [50] S. Fan, M. Ou, M. Scholten, Q. Li, Z. Shang, Y. Wang, J. Xu, H. Yang, I. M. Eremin, and H.-H. Wen, Superconducting gap structure and bosonic mode in $\text{La}_2\text{PrNi}_2\text{O}_7$ thin films at ambient pressure, [arXiv:2506.01788](https://arxiv.org/abs/2506.01788).
- [51] J. Shen, G. Zhou, Y. Miao, P. Li, Z. Ou, Y. Chen, Z. Wang, R. Luan, H. Sun, Z. Feng, X. Yong, Y. Li, L. Xu, W. Lv, Z. Nie, H. Wang, H. Huang, Y.-J. Sun, Q.-K. Xue, J. He, and Z. Chen, Nodeless superconducting gap and electron-boson coupling in $(\text{La,Pr,Sm})_3\text{Ni}_2\text{O}_7$ films, [arXiv:2502.17831](https://arxiv.org/abs/2502.17831).
- [52] W. Sun, Z. Jiang, B. Hao, S. Yan, H. Zhang, M. Wang, Y. Yang, H. Sun, Z. Liu, D. Ji, Z. Gu, J. Zhou, D. Shen, D. Feng, and Y. Nie, Observation of superconductivity-induced leading-edge gap in Sr-doped $\text{La}_3\text{Ni}_2\text{O}_7$ thin films, [arXiv:2507.07409](https://arxiv.org/abs/2507.07409).
- [53] Q.-G. Yang, D. Wang, and Q.-H. Wang, Possible s_{\pm} -wave superconductivity in $\text{La}_3\text{Ni}_2\text{O}_7$, *Phys. Rev. B* **108**, L140505 (2023).
- [54] Y.-B. Liu, J.-W. Mei, F. Ye, W.-Q. Chen, and F. Yang, s^{\pm} -wave pairing and the destructive role of apical-oxygen deficiencies in $\text{La}_3\text{Ni}_2\text{O}_7$ under pressure, *Phys. Rev. Lett.* **131**, 236002 (2023).
- [55] Y. Gu, C. Le, Z. Yang, X. Wu, and J. Hu, Effective model and pairing tendency in the bilayer ni-based superconductor $\text{La}_3\text{Ni}_2\text{O}_7$, *Phys. Rev. B* **111**, 174506 (2025).
- [56] Y. Zhang, L.-F. Lin, A. Moreo, T. A. Maier, and E. Dagotto, Structural phase transition, s_{\pm} -wave pairing, and magnetic stripe order in bilayered superconductor $\text{La}_3\text{Ni}_2\text{O}_7$ under pressure, *Nat. Commun.* **15**, 2470 (2024).
- [57] J. Huang, Z. D. Wang, and T. Zhou, Impurity and vortex states in the bilayer high-temperature superconductor $\text{La}_3\text{Ni}_2\text{O}_7$, *Phys. Rev. B* **108**, 174501 (2023).
- [58] Y. Zhang, L.-F. Lin, A. Moreo, T. A. Maier, and E. Dagotto, Trends in electronic structures and s_{\pm} -wave pairing for the rare-earth series in bilayer nickelate superconductor $\text{R}_3\text{Ni}_2\text{O}_7$, *Phys. Rev. B* **108**, 165141 (2023).
- [59] Y. Wang, K.-Y. Jiang, Z. Wang, F.-C. Zhang, and J. Hu, Elec-

- tronic and magnetic structures of bilayer $\text{La}_3\text{Ni}_2\text{O}_7$ at ambient pressure, *Phys. Rev. B* **110**, 205122 (2024).
- [60] K.-Y. Jiang, Y.-H. Cao, Q.-G. Yang, H.-Y. Lu, and Q.-H. Wang, Theory of pressure dependence of superconductivity in bilayer $\text{La}_3\text{Ni}_2\text{O}_7$, *Phys. Rev. Lett.* **134**, 076001 (2025).
- [61] S. Wakimoto, K. Yamada, J. M. Tranquada, C. D. Frost, R. J. Birgeneau, and H. Zhang, Disappearance of antiferromagnetic spin excitations in overdoped $\text{La}_{2-x}\text{Sr}_x\text{CuO}_4$, *Phys. Rev. Lett.* **98**, 247003 (2007).
- [62] M. Le Tacon, G. Ghiringhelli, J. Chaloupka, M. M. Sala, V. Hinkov, M. W. Haverkort, M. Minola, M. Bakr, K. J. Zhou, S. Blanco-Canosa, C. Monney, Y. T. Song, G. L. Sun, C. T. Lin, G. M. De Luca, M. Salluzzo, G. Khaliullin, T. Schmitt, L. Braicovich, and B. Keimer, Intense paramagnon excitations in a large family of high-temperature superconductors, *Nature Physics* **7**, 725–730 (2011).
- [63] M. Wang, C. Zhang, X. Lu, G. Tan, H. Luo, Y. Song, M. Wang, X. Zhang, E. A. Goremychkin, T. G. Perring, T. A. Maier, Z. Yin, K. Haule, G. Kotliar, and P. Dai, Doping dependence of spin excitations and its correlations with high-temperature superconductivity in iron pnictides, *Nat. Commun.* **4**, 2874 (2013).
- [64] P. Dai, Antiferromagnetic order and spin dynamics in iron-based superconductors, *Rev. Mod. Phys.* **87**, 855–896 (2015).
- [65] M. Wang, B. Hao, W. Sun, S. Yan, S. Sun, H. Zhang, Z. Gu, and Y. Nie, Electron-hole crossover in $\text{La}_{3-x}\text{Sr}_x\text{Ni}_2\text{O}_{7-\delta}$ thin films (2025), [arXiv:2508.15284 \[cond-mat.supr-con\]](https://arxiv.org/abs/2508.15284).
- [66] X. Lu, W. Zhang, Y. Tseng, R. Liu, Z. Tao, E. Paris, P. Liu, T. Chen, V. N. Strocov, Y. Song, R. Yu, Q. Si, P. Dai, and T. Schmitt, Spin-excitation anisotropy in the nematic state of detwinned FeSe, *Nat. Phys.* **18**, 806–812 (2022).
- [67] S. Wakimoto, H. Zhang, K. Yamada, I. Swainson, H. Kim, and R. J. Birgeneau, Direct relation between the low-energy spin excitations and superconductivity of overdoped high- T_c superconductors, *Phys. Rev. Lett.* **92**, 217004 (2004).
- [68] D. J. Scalapino, A common thread: the pairing interaction for unconventional superconductors, *Rev. Mod. Phys.* **84**, 1383–1417 (2012).
- [69] H. Lu, M. Rossi, A. Nag, M. Osada, D. F. Li, K. Lee, B. Y. Wang, M. Garcia-Fernandez, S. Agrestini, Z. X. Shen, E. M. Been, B. Moritz, T. P. Devereaux, J. Zaanen, H. Y. Hwang, K.-J. Zhou, and W. S. Lee, Magnetic excitations in infinite-layer nickelates, *Science* **373**, 213–216 (2021).